ADVANCED ENERGY MATERIALS
www.advenergymat.de

A Stretchable Nanogenerator with Electric/Light Dual-Mode Energy Conversion

Huajing Fang, Xiandi Wang, Qiang Li, Dengfeng Peng, Qingfeng Yan, and Caofeng Pan**

As an alternative technology, stretchable electronics attract long-lasting attention. A newly-designed stretchable nanogenerator with unique dual-mode energy conversion is reported. The ability of converting the input mechanical stimuli to either electric or light output is achieved by monolithically integrating a transparent single-electrode triboelectric nanogenerator (S-TENG) with a ZnS based mechanoluminescence (ML) composite. This stretchable device with versatile functions promotes the development of the smart systems to efficiently and diversely utilize ubiquitous mechanical energy and demonstrates great potential for artificial e-skins.

1. Introduction

The massive development of modern electronics places new physical requirements on electronic components. Stretchable electronics have attracted long-lasting attentions as an alternative technology in the future.[1–3] Compared with the traditional rigid electronic devices, this new class of electronics that enables the applications on moveable parts and rugged surface has promoted the development in wearable devices and artificial intelligent electronic skins (e-skins).[4–8] Many impressive results have been achieved in recent years, ranging from transistors to stretchable displays and solid-state lighting systems.[9–13] However, a sustaining power source to drive these stretchable devices is highly desired but remains a challenge.

Harvesting the green and renewable energy from ambient environment is one promising solution for wireless and self-sustainable operation.[14–16] Compared to other outdoor renewable energy resources such as solar, wind, and thermal energy, harvesting mechanical energy is more attractive due to the extensive availability of the target resource.[17–19] The triboelectric nanogenerator (TENG) aiming to convert mechanical energy into electricity has shown a huge impact on the energy sector of the scientific community since the first demonstration in early 2012.[20] Benefiting from the high electric output, TENGs have been successfully used as a promising power source to drive devices such as sensors,[21–23] memories,[24,25] and electrochromic windows.[26] However, in most previous works, the TENGs were not suitable for powering wearable devices or e-skins, especially under a highly stretched condition.[27] Hence, improving the stretchability of TENG is one of the most critical issues to further expand its scope of application.[28,29]

On the other hand, mechanical energy can also make some materials illuminate directly without any electrical energy supply, defined as mechanoluminescence (ML). This feature may also provide extensive applications in the field of self-powered lighting and displays.[30] Metal-ion-doped ZnS has been widely regarded as one of the most effective candidates for ML.[31] Nonetheless, its applications have been quite limited by the lack of durability derived from the rigid nature as an inorganic material. Based on an ingenious strategy of embedding the micro/nanoscale phosphors in soft polymers, the resulting composites have been rapidly active in various areas during the past three years.[32–36] While the pursuit of multifunctionality has become a new important trend in these years, along with the intensive development on the microelectronic devices toward light weight, miniaturization, and integration.[37–39]

Here, we present the first stretchable device in which the two effects, TENG and ML, can be realized simultaneously. First, we developed a very simple fabrication process to get a polydimethylsiloxane (PDMS)-supported silver nanowires (Ag NWs) transparent and stretchable single-electrode TENG (S-TENG). With the periodic contact/separation motion between the PDMS film and finger pulp, the S-TENG can deliver a high electric output of open-circuit voltage V_{oc} = 70 V and short-circuit current density J_{sc} = 1.5 mA m^{-2}. By integrating this S-TENG with another PDMS-supported composite, it can transfer stress to the embedded ZnS powder efficiently which is qualified for bright ML. Since each layer of the device is intrinsically stretchable material, the entirety also shows an excellent mechanical robustness which guarantees the durability of the device. The novelty of this stretchable device lies in the ability of converting the input mechanical stimuli to either electric or light output, demonstrating its great potential for application in multifunctional wearable devices and artificial e-skins. With the unique

H. Fang, Prof. Q. Li, Prof. Q. Yan
Department of Chemistry
Tsinghua University
Beijing 100084, P. R. China
E-mail: yanqf@mail.tsinghua.edu.cn
X. Wang, Dr. D. F. Peng, Prof. C. F. Pan
Beijing Institute of Nanoenergy and Nanosystems
Chinese Academy of Sciences
National Center for Nanoscience and Technology (NCNST)
Beijing 100083, P. R. China
E-mail: cfpan@binn.cas.cn

DOI: 10.1002/aenm.201600829

 © 2016 WILEY-VCH Verlag GmbH & Co. KGaA, Weinheim

dual-mode conversion, this work may also open a window for efficient and diverse utilization of the mechanical energy.

2. Results and Discussion

The device structure of the stretchable single-electrode TENG proposed here is schematically illustrated in **Figure 1**a. The S-TENG is composed of Ag NWs transparent electrode sandwiched by two layers of PDMS film. A cross-section scanning electron microscopy (SEM) image of the device is shown in the inset of Figure 1a, which clearly demonstrates the sandwich structure. It also confirms that Ag is only distributed within a thickness of less than 1 μm between two pure PDMS films. Note that, the Ag NWs transparent electrode is a vital component in our hybrid device. It has emerged as the most promising candidate to meet the requirement of various flexible electronic devices, but has rarely been used in TENG.[40–44] The high conductivity even under a highly tensile strain makes it the best choice to carry out the functions of stretchable S-TENG here. Figure 1b shows the SEM image of Ag NWs electrode deposited on the PDMS substrate. The Ag NWs randomly oriented and uniformly distributed over the entire coated area to form a conductive network. Another worth-noting feature of the S-TENG is its superior optical transmittance. Figure 1c plots the transmittance of the S-TENG with an average value of 80% in a broad wavelength range from 350 to 800 nm. A photograph of the S-TENG is presented as the inset. The high transparency of the S-TENG is very conducive to integration with light emitting devices, as will be shown shortly.

The working principle of the fabricated S-TENG can be resolved as the coupling between contact electrification and electrostatic induction, more details can be found in Figure S1 in the Supporting Information. Briefly, charge transfer between the surfaces of skin and PDMS was accomplished when they fully contact with each other. According to the triboelectric series,[45–47] electrons are injected from finger pulp to the top PDMS film, leading to net negative charges ($-\sigma$) at the surface of PDMS. The produced triboelectric charges with opposite polarity (σ) are also screened on skin. Under the contact/separation motions,

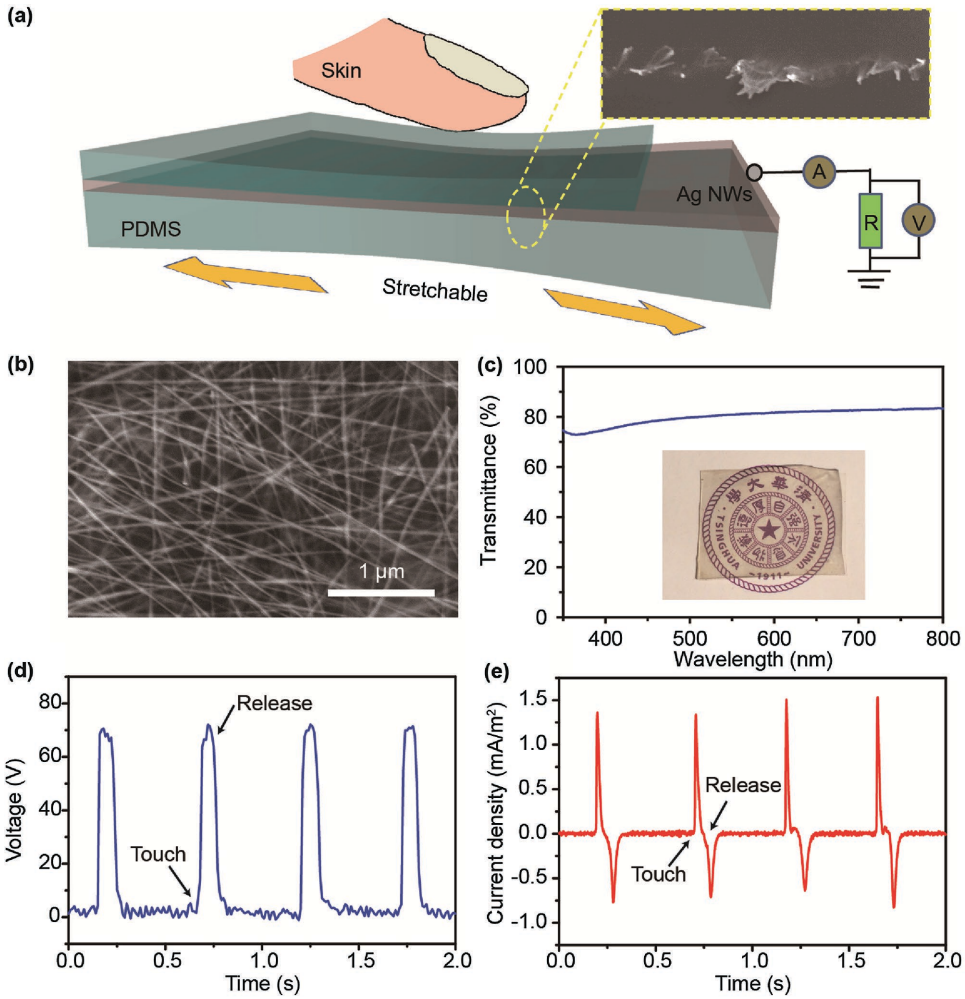

Figure 1. a) Schematic diagram of the stretchable single-electrode TENG. Inset is a cross-sectional SEM image of the S-TENG with a sandwich structure. b) SEM image of the Ag NWs coated on the PDMS surface. c) Optical transmittance of the stretchable S-TENG measured with a UV–vis spectrometer. The inset shows a photograph of the as-prepared stretchable S-TENG. d) The measured output voltage and (e) current density of the S-TENG during periodic contact/separation between the top PDMS film and finger pulp.

© 2016 WILEY-VCH Verlag GmbH & Co. KGaA, Weinheim

both the electric potential difference and induced current were caused by the free electrons transferring between the Ag NWs electrode and the ground. Figure 1d shows the measured open-circuit voltage (V_{oc}) between the Ag NWs electrode and ground by an electrometer with very large input resistance. The peak values of the V_{oc} were found to be ≈70 V during periodic contact/separation between the finger pulp and top PDMS film. The corresponding short-circuit current density (J_{sc}) output from the S-TENG reached 1.5 mA m^{-2}, as shown in Figure 1e. Moreover, the power delivered from the S-TENG during a full cycle of touching and releasing motions was able to instantaneously turn on 20 green LEDs (see Figure S2 and Video S1, Supporting Information). It visually presents that the produced energy can be directly used as an effective power source.

The S-TENG with sandwich structure we designed is a competent stretchable nanogenerator. To confirm that, it is necessary to evaluate the output performance of the S-TENG under different tensile strains. However, the randomness of human motions (touching/releasing here) always results in nonuniform output peak values of the TENG. This problem restricts us to finely and quantitatively study the effect of tensile strain on the performance of S-TENG. Hence, we deformed the S-TENG (original size 2 × 4 cm^2) with repeated compressive loading cycles generated by a linear motor to substitute the human finger touching. An aluminum foil (1 × 1 cm^2) was attached to the linear motor as the opposite friction material to contact with the S-TENG in this section. The electric potential difference between the Ag NWs electrode and the ground was recorded during the contact/separation motions. **Figure 2**a shows the output voltage of the S-TENG under different tensile strains ranging from 0% to 50%. As we can see, the output voltage changed little even under a highly stretched condition. The inset shows the photographs of a stretching test with a length increase of over 50%. The S-TENG can perfectly recover its original shape after releasing the tensile force. A comparison of the output voltage peak at the initial state and stretched state (50% strain) is presented in Figure 2b. The stability of this S-TENG is also a very important property in determining the possible applications. The performance of our S-TENG exhibits virtually no loss after 1000 times stretching–releasing (S–R) cycles with 30% strain, as shown in Figure 2c. In theory, the S-TENG would not invalid until the tensile strain destroyed the stretchable Ag NWs electrode. As we know from the working principle of this S-TENG, Ag NWs electrode is the key part in electrostatic induction process. So we investigated the change of resistance of Ag NWs electrode with various tensile strains. After clamping the S-TENG by two fixtures connected to the current–voltage (I–V) measurement system, the sample was stretched to specific lengths by a mechanical equipment. As shown in Figure 2d, the I–V characteristics of the Ag NWs electrode in the S-TENG exhibit an Ohmic behavior regardless of the applied strains. The current decreases monotonically with the increase of the tensile strain. The inset plots the relative change of the resistance under different tensile strains. The resistance of Ag NWs electrode only changed five times even when the S-TENG was stretched up to 50% tensile strain. The superior mechanical stability of the Ag NWs electrode was attributed to two major structural strategies. Firstly, the Ag

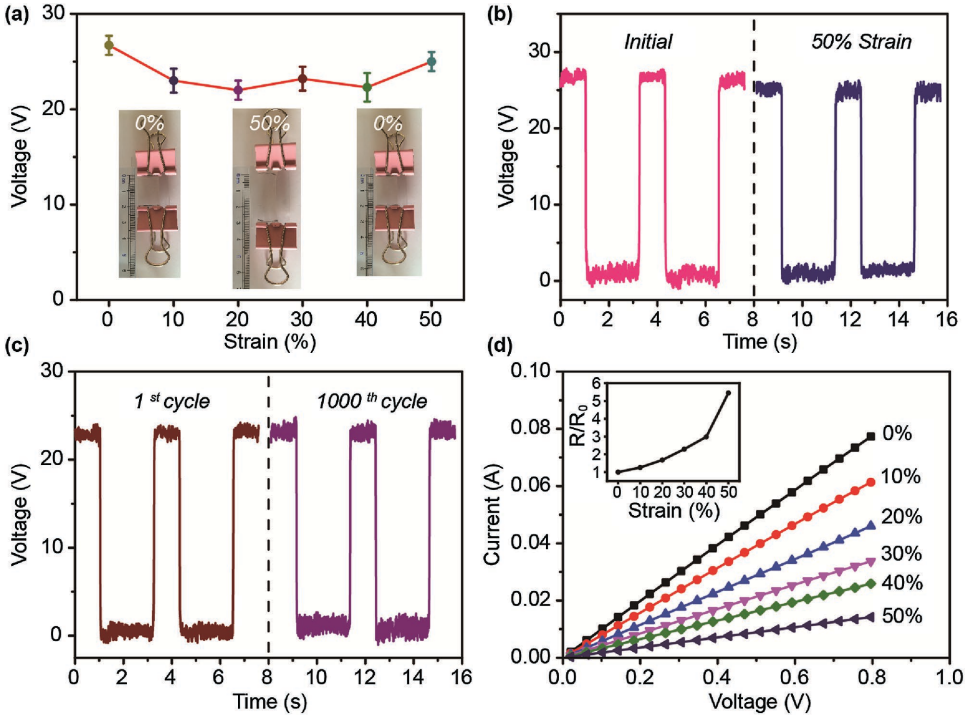

Figure 2. a) The output voltage of the S-TENG under various tensile strains. The inset shows the photographs of a stretching test with a length increase of 50%. b) The comparison of the output voltage under the initial state and stretched state (50% strain). c) The output voltage at 30% strain when the S-TENG has been operated for 1 and 1000 cycles. d) Current–voltage curves of the S-TENG under different levels of strain, the inset is the relative change in the resistance as a function of tensile strain.

© 2016 WILEY-VCH Verlag GmbH & Co. KGaA, Weinheim

NWs are uniformly distributed to form a conductive network, thus can accommodate the deformation more effectively by changing the network shapes.[48] Secondly, the sandwich structure of the S-TENG is also an advantage. As we know, the compressive stress in the transverse direction of stretching will make Ag NWs detach and buckle out of plane permanently.[49] In this work, the top PDMS was coated on the exposed Ag NWs electrode as a capping layer. This capping layer can constrain the embedded Ag NWs network so that the conductivity can be maintained under the stretching–releasing operations. Thus, the change of orientations and positions of Ag NWs in the sandwich structure can be based on an affine transformation.[50]

In order to realize the dual-mode energy conversion, we integrated the S-TENG with another PDMS-supported ML composites. The integration process was achieved by simply embedding ZnS:Al,Cu powder in the bottom PDMS polymer matrix. **Figure 3**a shows the structure of the integrated device. The cross-sectional SEM image of the integrated device was observed to confirm the mixed state nature of the ZnS:Al,Cu powder and the PDMS polymer matrix. As shown in Figure 3b, the ZnS:Al,Cu powder have been well dispersed in the PDMS matrix without any bubbles and voids. Notably, the dense filling is essential for high-brightness device because intense ML can only be obtained with high durable materials. Although PDMS is an efficient stress-transferring medium with robust characteristics, the existence of bubbles and voids in composite will lead to the rupture during the high degree of stretching vibration. The phase structure of the filled ZnS:Al,Cu powder was characterized by the X-ray diffraction as shown in Figure 3c. The sharp peaks are consistent with the planes of hexagonal wurtzite structure. The wurtzite-type ZnS with the space group of *P63mc* is of noncentral symmetric structure, as the inset atomic model shown. The lack of symmetry center makes it exhibit a more sensible piezoelectricity. It has been demonstrated in previous works that the piezoelectric potential is capable of triggering the luminescent center of metal-ion dopants, leading to the light emissions of the composites under external strain.[35,36,51] Figure 3d is a high-magnification cross-sectional SEM image at the interface between ML composite and pure PDMS. A layer of Ag NWs electrode embedded here can be clearly seen, which carries out the function of S-TENG. The superior optical transmittance of the Ag NWs electrode allowed the bidirectional light emission of the integrated device, as visually presented in Figure 3e.

Next, we investigated the optical output characteristics of the integrated device. A custom-built set of stretching machine was designed for the dynamical S–R motions (see Figure S3, Supporting Information). The strain and frequency can be readily modulated by a linear motor. When applying a fixed strain of 25% to the sample, the ML spectra with different S–R frequency from 1 to 5 Hz are shown in **Figure 4**a. The dominant peak of the luminescence spectrum is seen at 510 nm, which can be understood by the donor–acceptor (D–A) type emission process. The Al^{3+} substitution to Zn^{2+} site (Al_{Zn}) can generate a donor level below the conduction band, while the acceptor level above the valance band was caused by the Cu^{+} substitution to Zn^{2+} site (Cu_{Zn}). As aforementioned, carriers in the luminescent center of metal-ion-doped ZnS can be excited to a higher energy level by the piezoelectric potential. And the luminescence is induced by the subsequent electron–hole (e–h) recombination. Thus, the dominant peak at 510 nm can be explained from the D–A recombination of Al_{Zn}-Cu_{Zn} in this work. The emission intensity against the S–R frequency is plotted in the inset of Figure 4a. The experimental results suggest that ML

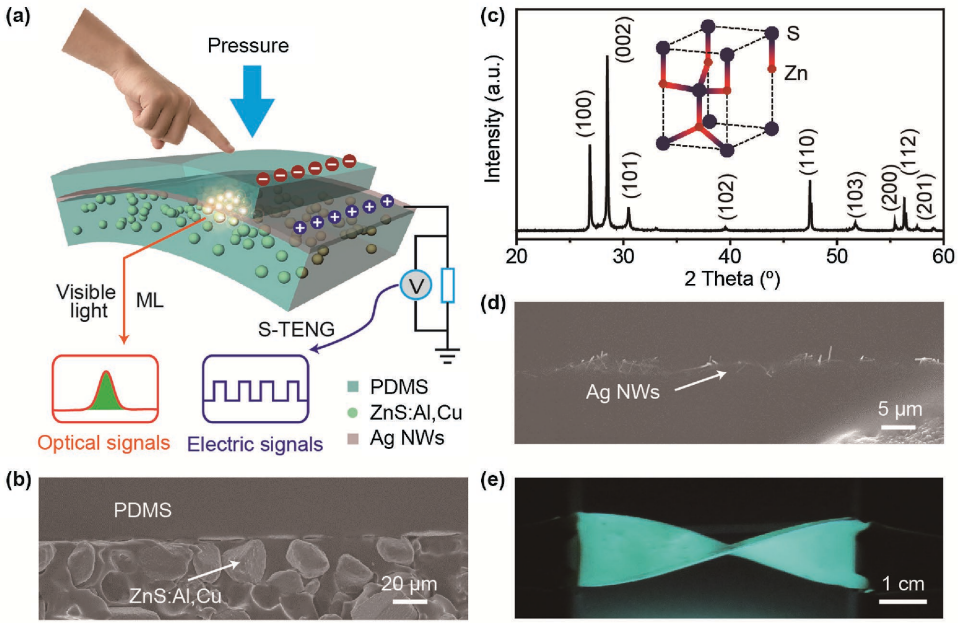

Figure 3. a) The schematic structure of an integrated device. b) A cross-sectional SEM image of the integrated device. c) X-ray diffraction (XRD) pattern of ZnS:Al,Cu powder, showing a typical wurtzite structure (JCPDS card no. 36-1450). The inset shows the atomic model of the wurtzite ZnS. d) A magnified cross-sectional SEM image at the interface between ML composite and pure PDMS. e) The photograph of a twisting device showing the flexibility and bidirectional light emission under a low intensity UV light ($\lambda = 365$ nm).

© 2016 WILEY-VCH Verlag GmbH & Co. KGaA, Weinheim

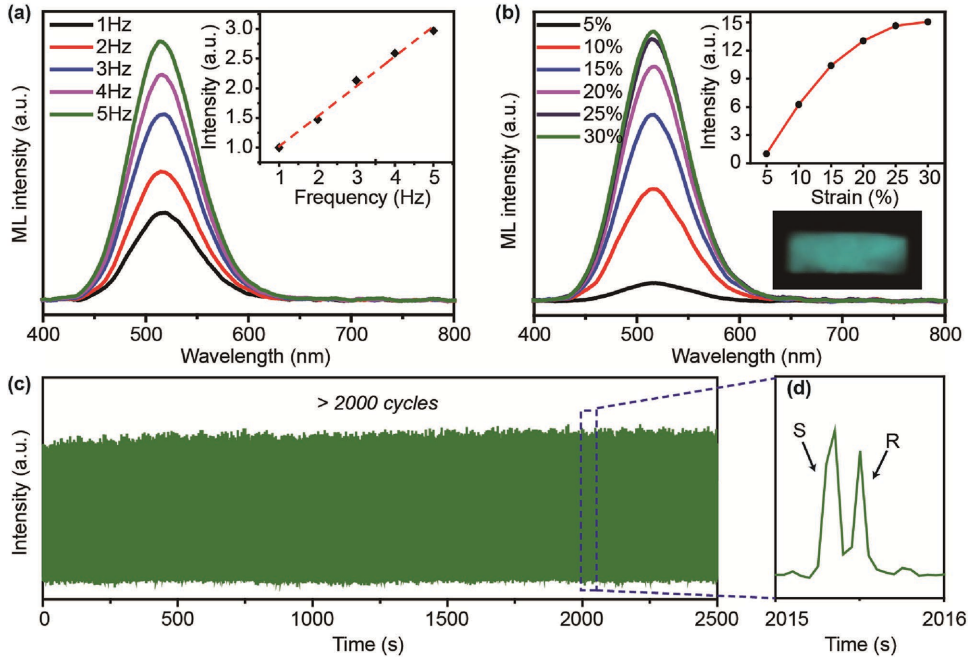

Figure 4. Optical characteristics of the integrated device during S–R motions. a) The ML spectra of the integrated device with increasing S–R frequency. b) The ML spectra of the integrated device with increasing strain. The upper inset illustrates the relationship between the ML intensity and strain. The lower inset is a photograph of the S–R motion-induced ML. c) Stability and repeatability test of the ML in the integrated device for more than 2000 cycles. d) The enlarged view of the time response ML spectra during one S–R motions.

intensity of the integrated device is linearly dependent on the S–R frequency. As shown in Figure 4b, driven with a fixed frequency of 4 Hz, the luminance also increased with the increasing strain. But it is a nonlinear relationship between the ML intensity and strain with a saturated trend, as shown in the upper inset. This bright green emission can be seen by the naked eyes. The lower inset shows a photograph of the device with S–R motion-induced ML. In addition, the Commission Internationale de L'Eclairage (CIE) coordinate of the ML in the integrated device was observed to be (0.1844, 0.3642). It corresponds to a typical green emission, details can be found in Figure S4, Supporting Information.

The high durability of ML is another important characteristic for the practical applications of this integrated devices. To confirm the durability in repeated S–R conditions, we measured the continuous ML intensity for more than 2000 cycles. The integral intensity over 450–600 nm was plotted versus time. As shown in Figure 4c, the integrated device displays a consistent ML intensity without any performance degradation throughout the whole test. Furthermore, Figure 4d shows the enlarged view of the output ML signals over a single cycle. The ML intensity shows a typical double-peak in each cycle, corresponding to the twice emissions in stretching and releasing steps respectively. The visual details of the S–R motions induced ML during a few cycles can also be clearly observed in Video S2, Supporting Information.

3. Conclusion

In summary, we have introduced a stretchable nanogenerator with the unique dual-mode energy conversion for the first time. It can convert the input mechanical stimuli to either electric or light output by monolithically integrating a transparent S-TENG with a ZnS based mechanoluminescence composites. The stretchable and skin-friendly S-TENG is made of an Ag NWs network electrode sandwiched by two layers of PDMS film. The working principle is based on the charge transfer between the ground and the transparent Ag NWs electrode by utilizing the contact/separation motions between human skin and the PDMS film. The S-TENG can convert mechanical energy into electricity with a high output of V_{oc} = 70 V and J_{sc} = 1.5 mA m^{-2}. Meanwhile, the S-TENG exhibits a stable output performance even under a highly stretched condition. This approach provides a promising candidate for the stretchable and wearable power supplies. Furthermore, the integrated device displays a consistent ML intensity without any performance degradation in repeated S–R conditions of more than 2000 cycles. Our scalable strategies for stretchable device with multifunctions demonstrate a great potential for application to wearable devices and artificial e-skins.

4. Experimental Section

Materials and Devices Fabrication: Ag NWs were purchased from Nanjing XFNANO Materials Tech Co., Ltd. The Ag NWs were first dispersed in ethanol and sonicated for 10 min to minimize the agglomeration of nanowires. Then, the resulting solution was drop cast onto a pre-treated glass substrate at room temperature. A liquid PDMS (Sylgard 184 silicon elastomer, Dow Corning) prepolymer was prepared by mixing the base and cross-linking agent at a ratio of 10:1. After the Ag NWs were fully dried, the PDMS prepolymer was coated on them followed by evacuation to remove the air bubbles. Subsequent curing

© 2016 WILEY-VCH Verlag GmbH & Co. KGaA, Weinheim

was done at 90 °C for 2 h in a drying oven. Next, the Ag NWs/PDMS film (≈0.5 mm thick) was peeled off from the glass substrate and cut into rectangles (2 × 4 cm^2). The stretchable S-TENG was obtained by encapsulating the exposed Ag NWs with another layer of PDMS to form a sandwich structure. Silver paste was coated at the edges of the Ag NWs electrode as leads to the external electrical circuit. For integrated devices, the encapsulation layer of pure PDMS was substituted by an ML composite. This ML composite was prepared by uniformly mixed ZnS:Al,Cu powder (GGS42, Global Tungsten & Powders Co.) in PDMS prepolymer with a weight ratio of 7:3. The processes of evacuation and curing were similar with the previous steps. After curing, the integrated device was cut into rectangles (1.6 × 8 cm^2) before the ML characteristics, and the total thickness of the sample is about 1 mm.

Characterization: All the SEM images of the samples were taken on the field-emission scanning electron microscopy (JEOL JSM-6335F). The optical transmission of Ag NWs transparent electrode was measured using a UV–visible spectrophotometer (HITACHI, U-3010). The crystal structures of the ZnS:Al,Cu powder were characterized through X-ray diffraction (XRD, Bruker D8-Advance) using Cu Kα radiation. The *I–V* curves of the S-TENG under various tensile strains were measured by a digital sourcemeter (Keithley 2400). The output voltage and current density of the S-TENG were recorded by an electrometer with very large input resistance (Keithley 6514). A home-made measuring system was built to collect the optical characteristics of the integrated devices (details can be found in Figure S3, Supporting Information). The periodical S–R motion was controlled by a linear motor (Linmot E1100). ML spectra were recorded by a spectrometer (Ocean Optics QE65pro) in the range of 200–900 nm. CIE coordinates was measured by a spectroradiometer (PR-670, Photo Research Inc.).

Supporting Information

Supporting Information is available from the Wiley Online Library or from the author.

Acknowledgements

H.F. and X.W. contributed equally to this work. The authors are thankful for support from the "Thousand Talents" program of China for pioneering researchers and innovative teams and from the President Funding of the Chinese Academy of Sciences. This research was supported by the National key Basic Research Program of China (973 Program, Grant No. 2013CB632900), and the National Science Foundation of China (No. 51173097, 91333109, 51432005, 61405040, 61505010, and 51502018), Beijing City Committee of Science and Technology (Z151100003315010), Beijing Natural Science Foundation (2164077 and 2164076). The Tsinghua University Initiative Scientific Research Program (No. 20131089202) and the Open Research Fund Program of the State Key Laboratory of Low-Dimensional Quantum Physics (No. KF201516) are acknowledged for partial financial support.

Received: April 20, 2016
Revised: May 13, 2016
Published online:

[1] J. J. Liang, L. Li, X. F. Niu, Z. B. Yu, Q. B. Pei, *Nat. Photonics* **2013**, *7*, 817.
[2] C. Y. Yan, X. Wang, M. Q. Cui, J. X. Wang, W. B. Kang, C. Y. Foo, P. S. Lee, *Adv. Energy Mater.* **2014**, *4*, 1301396.
[3] Z. Q. Niu, H. B. Dong, B. W. Zhu, J. Z. Li, H. H. Hng, W. Y. Zhou, X. D. Chen, S. S. Xie, *Adv. Mater.* **2013**, *25*, 1058.
[4] D. J. Lipomi, M. Vosgueritchian, B. C.-K. Tee, S. L. Hellstrom, J. A. Lee, C. H. Fox, Z. N. Bao, *Nat. Nanotechnol.* **2011**, *6*, 788.
[5] B. C.-K. Tee, A. Chortos, A. Berndt, A. K. Nguyen, A. Tom, A. McGuire, Z. L. C. Lin, K. Tien, W. G. Bae, H. L. Wang, P. Mei, H.-H. Chou, B. X. Cui, K. Deisseroth, T. N. Ng, Z. N. Bao, *Science* **2015**, *350*, 313.
[6] S. Xu, Y. Zhang, L. Jia, K. E. Mathewson, K.-I. Jang, J. Kim, H. Fu, X. Huang, P. Chava, R. Wang, S. Bhole, L. Wang, Y. J. Na, Y. Guan, M. Flavin, Z. Han, Y. Huang, J. A. Rogers, *Science* **2014**, *344*, 70.
[7] R.-H. Kim, D.-H. Kim, J. Xiao, B. H. Kim, S.-I. Park, B. Panilaitis, R. Ghaffari, J. Yao, M. Li, Z. Liu, V. Malyarchuk, D. G. Kim, A.-P. Le, R. G. Nuzzo, D. L. Kaplan, F. G. Omenetto, Y. Huang, Z. Kang, J. A. Rogers, *Nat. Mater.* **2010**, *9*, 929.
[8] H. J. Fang, H. Tian, J. Li, Q. Li, J. Y. Dai, T. L. Ren, G. F. Dong, Q. F. Yan, *Nano Energy* **2016**, *20*, 48.
[9] Z. B. Yu, X. F. Niu, Z. T. Liu, Q. B. Pei, *Adv. Mater.* **2011**, *23*, 3989.
[10] A. Chortos, J. Lim, J. W. F. To, M. Vosgueritchian, T. J. Dusseault, T.-H. Kim, S. Hwang, Z. N. Bao, *Adv. Mater.* **2014**, *26*, 4253.
[11] M. S. White, M. Kaltenbrunner, E. D. Głowacki, K. Gutnichenko, G. Kettlgruber, I. Graz, S. Aazou, C. Ulbricht, D. A. M. Egbe, M. C. Miron, Z. Major, M. C. Scharber, T Sekitani, T. Someya, S. Bauer, N. S. Sariciftci, *Nat. Photonics* **2013**, *7*, 811.
[12] C. Larson, B. Peele, S. Li, S. Robinson, M. Totaro, L. Beccai, B. Mazzolai, R. Shepherd, *Science* **2016**, *351*, 1071.
[13] T. Sekitani, H. Nakajima, H. Maeda, T. Fukushima, T. Aida, K. Hata, T. Someya, *Nat. Mater.* **2009**, *8*, 494.
[14] S. Xu, Y. Qin, C. Xu, Y. G. Wei, R. S. Yang, Z. L. Wang, *Nat. Nanotechnol.* **2010**, *5*, 366.
[15] M. D. Han, X. S. Zhang, B. Meng, W. Liu, W. Tang, X. M. Sun, W. Wang, H. X. Zhang, *ACS Nano* **2013**, *7*, 8554.
[16] J. I. Sohn, S. N. Cha, B. G. Song, S. Lee, S. M. Kim, J. Y. Ku, H. J. Kim, Y. J. Park, B. L. Choi, Z. L. Wang, J. M. Kim, K. Kim, *Energy Environ. Sci.* **2013**, *6*, 97.
[17] G. Zhu, J. Chen, T. Zhang, Q. Jing, Z. L. Wang, *Nat. Commun.* **2014**, *5*, 3426.
[18] K. I. Park, C. K. Jeong, J. Ryu, G.-T. Hwang, K. J. Lee, *Adv. Energy Mater.* **2013**, *3*, 1539.
[19] K. I. Park, J. H. Son, G.-T. Hwang, C. K. Jeong, J. Ryu, M. Koo, I. Choi, S. H. Lee, M. Byun, Z. L. Wang, K. J. Lee, *Adv. Mater.* **2014**, *26*, 2514.
[20] F. R. Fan, Z. Q. Tian, Z. L. Wang, *Nano Energy* **2012**, *1*, 328.
[21] H. J. Fang, Q. Li, J. Ding, N. Li, H. Tian, L. J. Zhang, T. L. Ren, J. Y. Dai, L. D. Wang, Q. F. Yan, *J. Mater. Chem. C* **2016**, *4*, 630.
[22] Z. H. Lin, G. Cheng, Y. Yang, Y. S. Zhou, S. Lee, Z. L. Wang, *Adv. Funct. Mater.* **2014**, *24*, 2810.
[23] X. D. Wang, H. L. Zhang, L. Dong, X. Han, W. M. Du, J. Y. Zhai, C. F. Pan, Z. L. Wang, *Adv. Mater.* **2016**, *28*, 2896.
[24] X. Y. Chen, M. Iwamoto, Z. M. Shi, L. M. Zhang, Z. L. Wang, *Adv. Funct. Mater.* **2015**, *25*, 739.
[25] H. J. Fang, Q. Li, W. H. He, J. Li, Q. T. Xue, C. Xu, L. J. Zhang, T. L. Ren, G. F. Dong, H. L. W. Chan, J. Y. Dai, Q. F. Yan, *Nanoscale* **2015**, *7*, 17306.
[26] M. H. Yeh, L. Lin, P. K. Yang, Z. L. Wang, *ACS Nano* **2015**, *9*, 4757.
[27] K. N. Kim, J. Chun, J. W. Kim, K. Y. Lee, J.-U. Park, S.-W. Kim, Z. L. Wang, J. M. Baik, *ACS Nano* **2015**, *9*, 6394.
[28] F. Yi, L. Lin, S. M. Niu, P. K. Yang, Z. N. Wang, J. Chen, Y. S. Zhou, Y. L. Zi, J. Wang, Q. L. Liao, Y. Zhang, Z. L. Wang, *Adv. Funct. Mater.* **2015**, *25*, 3688.
[29] P.-K. Yang, L. Lin, F. Yi, X. H. Li, K. C. Pradel, Y. L. Zi, C.-I. Wu, J.-H. He, Y. Zhang, Z. L. Wang, *Adv. Mater.* **2015**, *27*, 3817.
[30] D. F. Peng, B. Chen, F. Wang, *ChemPlusChem* **2015**, *80*, 1209.
[31] C. N. Xu, T. Watanabe, M. Akiyama, X. G. Zheng, *Appl. Phys. Lett.* **1999**, *74*, 1236.
[32] S. M. Jeong, S. Song, S.-K. Lee, B. Choi, *Appl. Phys. Lett.* **2013**, *102*, 051110.
[33] S. M. Jeong, S. Song, S.-K. Lee, N. Y. Ha, *Adv. Mater.* **2013**, *25*, 6194.
[34] S. M. Jeong, S. Song, K.-I Joo, J. Kim, S.-H. Hwang, J. Jeong, H. Kim, *Energy Environ. Sci.* **2014**, *7*, 3338.

© 2016 WILEY-VCH Verlag GmbH & Co. KGaA, Weinheim

[35] M.-C. Wong, L. Chen, M.-K. Tsang, Y. Zhang, J. H. Hao, *Adv. Mater.* **2015**, *27*, 4488.
[36] X. D. Wang, H. L. Zhang, R. M. Yu, L. Dong, D. F. Peng, A. H. Zhang, Y. Zhang, H. Liu, C. F. Pan, Z. L. Wang, *Adv. Mater.* **2015**, *27*, 2324.
[37] Q. W. Zhang, K. Chen, L. L. Wang, H. Q. Sun, X. S. Wang, X. H. Hao, *J. Mater. Chem. C* **2015**, *3*, 5275.
[38] X. Pu, L. X. Li, M. M. Liu, C. Y. Jiang, C. H. Du, Z. F. Zhao, W. G. Hu, Z. L. Wang, *Adv. Mater.* **2016**, *28*, 98.
[39] L. B. Huang, G. X. Bai, M.-C. Wong, Z. B. Yang, W. Xu, J. H. Hao, *Adv. Mater.* **2016**, *28*, 2744.
[40] J. X. Wang, C. Y. Yan, K. J. Chee, P. S. Lee, *Adv. Mater.* **2015**, *27*, 2876.
[41] H. Lee, K. Lee, J. T. Park, W. C. Kim, H. Lee, *Adv. Funct. Mater.* **2014**, *24*, 3276.
[42] W. Gaynor, G. F. Burkhard, M. D. McGehee, P. Peumans, *Adv. Mater.* **2011**, *23*, 2905.
[43] S. Hong, H. Lee, J. Lee, J. Kwon, S. Han, Y. D. Suh, H. Cho, J. Shin, J. Yeo, S. H. Ko, *Adv. Mater.* **2015**, *27*, 4744.
[44] L. B. Hu, H. S. Kim, J.-Y. Lee, P. Peumans, Y. Cui, *ACS Nano* **2010**, *4*, 2955.
[45] J.-H. Lee, R. Hinchet, T. Y. Kim, H. Ryu, W. Seung, H.-J. Yoon, S.-W. Kim, *Adv. Mater.* **2015**, *27*, 5553.
[46] Z. L. Wang, *ACS Nano* **2013**, *7*, 9533.
[47] Y. Yang, H. L. Zhang, Z. H. Lin, Y. S. Zhou, Q. S. Jing, Y. J. Su, J. Yang, J. Chen, C. G. Hu, Z. L. Wang, *ACS Nano* **2013**, *7*, 9213.
[48] P. Lee, J. Lee, H. Lee, J. Yeo, S. Hong, K. H. Nam, D. Lee, S. S. Lee, S. H. Ko, *Adv. Mater.* **2012**, *24*, 3326.
[49] M. Amjadi, A. Pichitpajongkit, S. Lee, S. Ryu, I. Park, *ACS Nano* **2014**, *8*, 5154.
[50] B. Hu, N. Hu, Y. Li, K. Akagi, W. Yuan, T. Watanabe, Y. Cai, *Nanoscale Res. Lett.* **2012**, *7*, 402.
[51] L. Chen, M.-C. Wong, G. X. Bai, W. J. Jie, J. H. Hao, *Nano Energy* **2015**, *14*, 372.

© 2016 WILEY-VCH Verlag GmbH & Co. KGaA, Weinheim